

# 17 Super-QMC: Strong Coupling Perturbation for Lattice Models

Alexander Lichtenstein

I. Institut für Theoretische Physik

Universität Hamburg, 20355 Hamburg

## Contents

<b>1 Idea of reference system</b>	<b>2</b>
1.1 Generic Hamiltonian . . . . .	5
<b>2 Numerically exact lattice QMC</b>	<b>6</b>
2.1 Hirsch-Fye DQMC . . . . .	6
2.2 Continuous-time QMC . . . . .	7
<b>3 The DF-QMC method</b>	<b>8</b>
3.1 Real-space scheme . . . . .	8
3.2 $k$ -space scheme . . . . .	12
<b>4 Results for <math>8 \times 8</math> lattices</b>	<b>15</b>
<b>5 Discussion</b>	<b>19</b>

## 1 Idea of reference system

In this lecture we give an introduction to the theoretical description of interacting electron systems based on non-perturbative, strong-coupling expansions around optimal reference system. Density Functional Theory (DFT) and its Local Density Approximation (LDA) is based on the simplest reference system related with a homogeneous electron gas with constant external potential with the same Coulomb electron-electron interactions (see Fig. 1). Such a reference system can be solved via a numerically exact diffusion Monte Carlo scheme for the ground state energy as a function of electron density [1]. On other hand, the Dynamical Mean-Field Theory (DMFT) [2] for strongly interacting fermionic systems is based on a strong coupling expansion around an effective impurity reference system (Fig. 1). This scheme become exact in the limit of infinite lattice dimension [3].

In the finite lattice dimension we can start from the DMFT reference system and use an analytical perturbation for non-local correlation effects. The frequency dependent effective impurity DMFT problem nowadays can be efficiently solved within continuous time quantum Monte Carlo (CT-QMC) schemes [4]. Therefore the perturbation theory needs to be formulated in the action path integral formalism. We discuss here a general way to include correlations beyond the reference system [5] which is based on the dual-fermion path-integral formalism [6].

For DMFT an effective impurity model, tailored to the problem of strong correlations, serves as the reference system, see Fig. 1. Since in the zeroth-order of this perturbative expansion, i.e., on the level of the DMFT problem, we already have an interacting problem and since the perturbation is momentum and frequency dependent, one is forced to replace the Hamiltonians by actions within the path-integral formalism. Note that the fermion path integral can also be used to formulate the DMFT itself [2]. The dual-fermion approach is not necessarily bound to a specific starting point.

We recently developed a strong-coupling perturbation scheme for generic Hubbard models around a half-filled particle-hole-symmetric reference system, which is free from the fermionic sign problem [7]. The approach is based on the lattice determinant quantum Monte Carlo (QMC) method in continuous and discrete time for large periodic clusters in a fermionic bath. Considering the first-order perturbation in the shift of the chemical potential and of the second-neighbor hopping gives an accurate electronic spectral function for a parameter range corresponding to the optimally doped cuprate system for temperatures of the order of  $T/t=0.1$ , the region hardly accessible for straightforward lattice QMC calculations. We discuss the formation of a pseudogap and the nodal-antinodal dichotomy for doped Hubbard systems in the strong-coupling regime with interaction parameter  $U$  equal to the bandwidth and the optimal value of the next-nearest-neighbor hopping parameter  $t'$  for high-temperature superconducting cuprates. Extensive investigation of the fermionic sign problem in the lattice DQMC for the  $t-t'-U$  Hubbard model for  $U/t = 6$ ,  $t'/t = -0.2$  and its relation with a quantum critical point [8] gives the generic “sign” phase diagram presented in Fig. 2. The red region in the temperature-doping (chemical potential) diagram presents an “unacceptable” sign problem, where one can not do any accurate simulations. It is interesting that the  $d$ -wave superconducting dome lies exactly in-

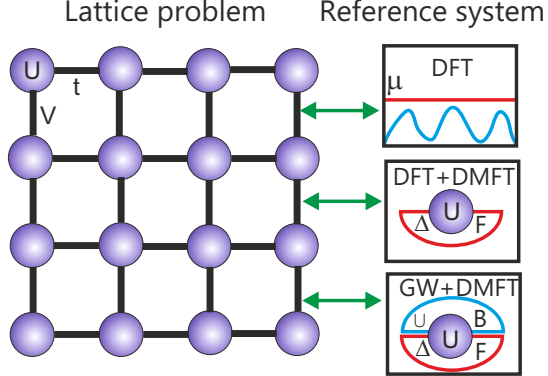


**Fig. 1:** Schematic representation of reference systems in many-body approaches to lattice-fermion models: (i) Density-functional theory (DFT) with the interacting homogeneous electron gas as a reference system, defined by a constant external potential  $\mu$ . (ii) Dynamical mean-field theory (DMFT) with an effective impurity problem as a reference system, defined by a fermionic bath, specified by the hybridization function  $\Delta$ . (iii) GW+DMFT with a correlated atom in a fermionic ( $\Delta$ ) and a bosonic bath ( $\Lambda$ ) due to effects of the frequency-dependent screening of long-range Coulomb ( $V$ ) interactions.

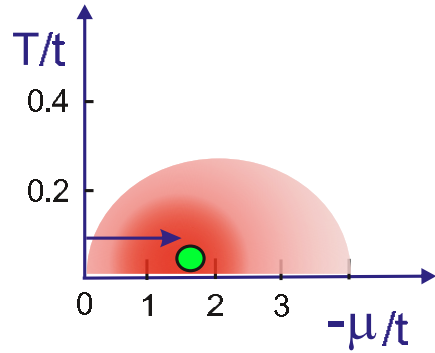


**Fig. 2:** Schematic representation of the sign-problem in QMC lattice-fermion calculations. The green circle shows the approximate position of maximum  $d$ -wave superconductivity with 15% hole doping. The blue arrow give the “direction” of the reference system approach.

side the “red-region”. The arrow gives the directions which we would like to pursue in order to overcome the sign problem. We will start from the sign-free half-field particle-hole symmetric case with  $\mu=0$  and move closer to the quantum critical point related with  $d$ -wave superconductivity in the cuprates. Comparing the density of states in Fig. 3 for the undoped case with a pseudogap, which is free from the sign-problem, and the hole doped case with  $\mu/t=-2$  with  $t'/t=-0.3$  with a very sharp peak at the Fermi level, one can understand that a non-trivial reason for the sign-problem may be related with a strong anomaly in the many-body spectrum.

The search for numerically exact solutions of the  $t-t'-U$  Hubbard model in the thermodynamic limit at arbitrary interaction strength, long-range hopping and doping  $\delta$  or, equivalently, chemical potential  $\mu$  at low temperature  $T=1/\beta$  is tremendously difficult. Modern computational approaches, based on lattice determinant quantum Monte Carlo (QMC) methods have made tremendous progress in the half-filled case without  $t'$  [9], but face an unacceptable fermionic sign problem for the general doped case related to the high-temperature superconductivity

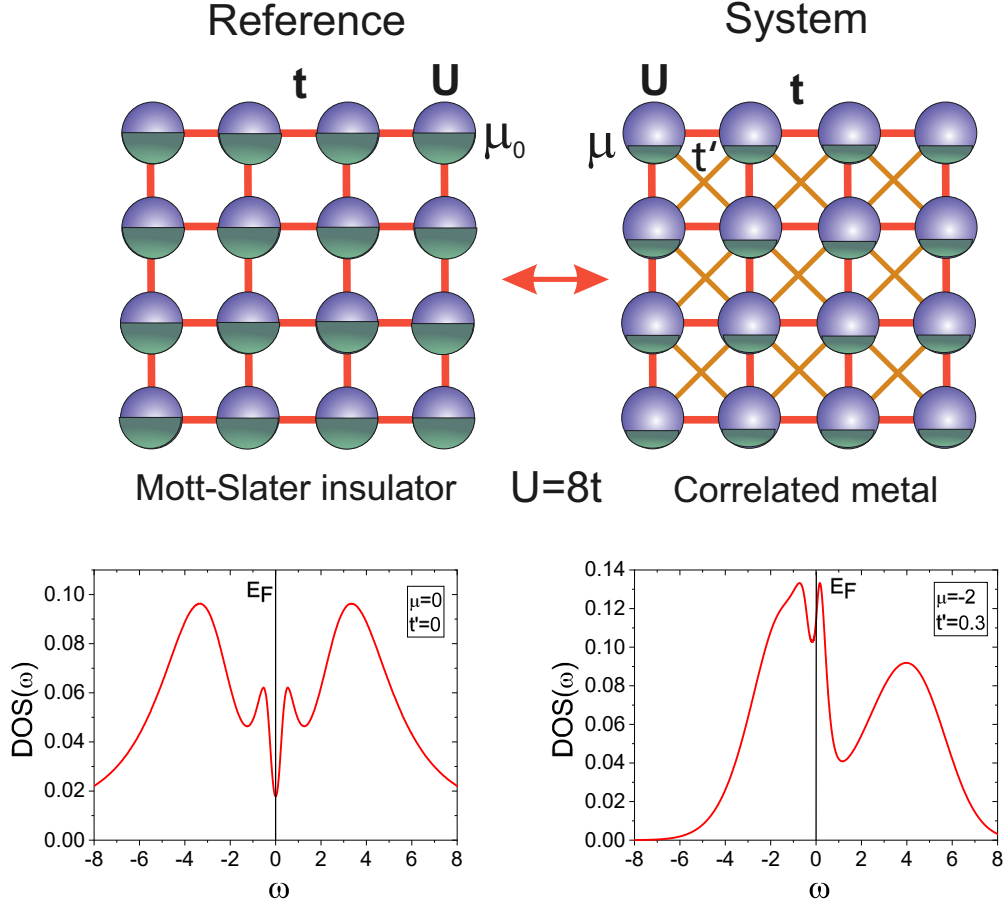


**Fig. 3:** Schematic representation of a half-filled reference system for the doped square lattice. Below: calculated density of states (DOS) in presented scheme for  $U/t = 8$ , Left: undoped case  $\mu = 0$  with  $t' = 0$ , Right: doped case  $\mu = -2$  with  $t'/t = -0.3$

(HTSC) problem, which is the main factor restricting the accuracy of QMC calculations for interacting fermion systems [10–12, 8]. A very important and largely unresolved problem is related to the next-nearest-neighbor hopping  $t'$  in the Hubbard model and its role in superconductivity [13–19]. There are two recent successful attempts to resolve this long-standing problem using zero-temperature a variational QMC scheme for realistic HTSC systems [20] in combination with DMRG for the  $t-t'-U$  Hubbard model on a large ribbon geometry [21].

On the other hand, a new class of diagrammatic Monte Carlo scheme [22] is claimed to have a “sign blessing” property which helps to reduce the effects of high-order diagrams. The state-of-the-art diagrammatic Monte Carlo scheme in the connected determinant mode (C-DET) [23], based on efficient Continuous Time Quantum Monte Carlo(CT-QMC) scheme in the weak coupling technique (CT-INT) [24], gives unprecedented accuracy for the doped Hubbard model [25, 26]. It becomes possible to study the formation of the pseudogap already at the beginning of the strong coupling case with  $U/t=6$  [25]. Nevertheless, the exponential convergence of the C-DET scheme for weak interactions [27, 28] turns into a divergence at large  $U$  values due to poles in the complex  $U$ -plane [26]. This means that calculations for interactions close to the bandwidth  $U/t \approx 8$  and temperature  $T/t \approx 0.1$  are still within a prohibited area in the phase diagram [26].

There is a recent interesting attempt to use a dynamical variational QMC scheme for the doped Hubbard model [29, 30], which gives a very reasonable description of the spectral function. The existence of the pseudogap can be explained in a simple model of electron fractionalization and the appearance of “dark” fermions which is supported by  $2\times 2$  cluster Dynamical Mean Field Theory (C-DMFT) [31, 17]. Moreover, the experimental RIXS spectra [32] of doped cuprate materials can be interpreted in such a theoretical model of the pseudogap formation. Larger clusters in the C-DMFT scheme for the doped case have, however, an unacceptable fermionic sign problem within the QMC scheme.

Here we discuss a different route to tackle the “sign problem” in the determinant lattice QMC scheme and design a strong-coupling perturbative solution for a general Hubbard model. The starting point is related to the “reference system” idea [33] which is basically quite simple and straightforward. The conventional choice of the noninteracting Hamiltonian as the reference system for the perturbation [34] is motivated by Wick’s theorem which allows to calculate exactly any many-particle Green functions: they are all expressed in terms of single-particle Green functions. The choice of a single-site approximation like dynamical mean-field theory [35] as the reference system leads to the dual fermion technique [6, 33]. Actually, the reference system can be arbitrary, assuming that we can calculate its Green functions of arbitrary order. It is worthwhile to mention here the very successful Peierls-Feynman-Bogoliubov variational principle [36–38]. In this case, a good variational estimate of the system’s free energy  $F$  with the Hamiltonian  $H_1$  is achieved on an optimal reference system with the Hamiltonian  $H_0$ , namely  $F_1 \leq F_0 + \langle H_1 - H_0 \rangle_0$ . One can hope therefore that even first-order corrections to the properly chosen reference system will already give a rich and adequate enough physical picture.

## 1.1 Generic Hamiltonian

The simplest model describing interacting fermions on a lattice is the single band Hubbard model, defined by the Hamiltonian

$$\hat{H}_\alpha = - \sum_{i,j,\sigma} t_{ij}^\alpha c_{i\sigma}^\dagger c_{j\sigma} + \sum_i U \left( n_{i\uparrow} - \frac{1}{2} \right) \left( n_{i\downarrow} - \frac{1}{2} \right) \quad (1)$$

where  $t_{ij}$  are hopping matrix elements including the chemical potential  $\mu$  in the diagonal part

$$t_{ij}^\alpha = \begin{cases} t & \text{if } i \text{ and } j \text{ are nearest neighbors,} \\ \alpha t' & \text{if } i \text{ and } j \text{ are next-nearest neighbors,} \\ \alpha \mu & \text{if } i = j, \\ 0 & \text{otherwise,} \end{cases} \quad (2)$$

and  $n_{i\sigma} = c_{i\sigma}^\dagger c_{i\sigma}$ . We introduce a “scaling” parameter  $\alpha=0, 1$ , which distinguishes a reference system  $H_0$  for  $\alpha=0$  and corresponds to the half-filled Hubbard model ( $\mu_0=0$ ) with only nearest neighbors hopping ( $t'_0=0$ ) from the final system  $H_1$  for  $\alpha=1$  with given  $\mu$  and  $t'$ . Note that long-range hoping parameters can be trivially included in the present formalism similar to  $t'$ .

The reference system now corresponds to the half-filled ( $\mu=0$ ) particle-hole symmetric ( $t'=0$ ) case (Fig. 3), where lattice Monte Carlo has no sign problem and the numerically exact solution for any practical value of  $U$  is possible within a broad range of temperatures [39]. Then we apply the lattice dual fermion perturbation theory [6,5,33] to find the first-order perturbative corrections in  $\mu$  and  $t'$ . To this end, it is sufficient to calculate the two-particle Green function, or, equivalently, the four-leg vertex, which can be done with sufficient accuracy within continuous time quantum Monte Carlo. Our reference system already has the main correlation effects in the lattice and shows the characteristic “four-peak” structure [40] with high-energy Hubbard bands around  $\pm U/2$  and antiferromagnetic Slater bands close to the insulating gap (which can be seen in the density of states in figure 3, left panel). After the dual fermion perturbation scheme correlated metallic states with the DMFT-like “three peak” structure appear with a pseudogap-like feature at high temperature (the density of states in figure 3, right panel). Results for the strong-coupling case ( $U=W=8t$ ) with practically interesting values of the chemical potential and next-nearest-neighbor hoppings corresponding to cuprate superconductors have shown the formation of a pseudogap and a nodal-antinodal dichotomy (that is, well-defined quasiparticles in the nodal part of the Fermi surface and strong quasiparticle damping for the antinodal part), which gives this approximation a perspective for practical applications.

## 2 Numerically exact lattice QMC

We briefly introduce here the main ideas of two different lattice QMC approaches for large periodic clusters in a bath. The first is based on the Hubbard-Stratonovich transformation of the local interaction in Eq. (2), the other is related with the continuous-time interaction (CT-INT) expansion scheme. Both QMC methods are used here for practical computations.

### 2.1 Hirsch-Fye DQMC

We use a path-integral formalism with Grassmann variables  $[c_i^*, c_i]$ . The space-time bare Green function  $\mathcal{G}_{ij}$  describes the non-interacting part of the Hamiltonian in Eq. (2) for  $N_x \times N_y$  2D-space ( $N = N_x \cdot N_y$ ) and  $L \times L$  discretized times in an effective bath representing the external infinite lattice with space-time index here  $i \equiv (\mathbf{r}, \tau)$ . Imaginary time slicing corresponds to the mesh  $\tau = l * \Delta\tau$  with  $l = 0, \dots, L-1$  and  $\Delta\tau = \beta/L$  with inverse temperature  $\beta$ . The interaction part of the Hamiltonian Eq. (2) is decoupled by mapping to auxiliary Ising fields  $s_i$  via a discrete Hirsch-Hubbard-Stratonovich transformation [41]

$$\exp(-U\Delta\tau(n_{i\uparrow}n_{i\downarrow} - (n_{i\uparrow} + n_{i\downarrow})/2)) = \frac{1}{2} \sum_{s_i=\pm 1} \exp(\lambda s_i(n_{i\uparrow} - n_{i\downarrow})), \quad (3)$$

where  $\lambda = \text{arccosh}(e^{U\Delta\tau/2})$  and for the best convergence of DQMC one uses the following “rule of thumb”  $U\Delta\tau/2 \lesssim 1$ . Then the effective lattice action become Gaussian

$$S[c^*, c] = - \sum_{i,j,\sigma} c_{i\sigma}^* G_{ij\sigma}^{-1} c_{j\sigma} \quad \text{with} \quad G_{ij\sigma}^{-1}(s) = \mathcal{G}_{ij\sigma}^{-1} - \delta_{i,j} \lambda s_i \sigma, \quad (4)$$

where  $s \equiv \{s_i\}$  with  $i = 1, \dots, N \cdot L$ . Note that in time space the delta function should be anti-periodic for fermions [42, 43, 2] and Eq. (4) has a schematic form. For such a Gaussian action we can integrate-out fermionic the degrees of freedom and get for the partition function the following formula used in the determinant QMC scheme

$$Z = \frac{1}{2^{NL}} \sum_s \prod_{\sigma} \det[G_{\sigma}^{-1}(s)], \quad (5)$$

where the sum over Ising auxiliary fields  $s_i$  performed with an importance-sampling Monte Carlo algorithm with probability  $P(s) = \det[G_{\uparrow}^{-1}(s)] \cdot \det[G_{\downarrow}^{-1}(s)]$  which is always positive for the half-field particle-hole symmetric Hubbard model [42]. Within the DQMC scheme the exact single-particle Green function of the reference system can be calculated as

$$g_{ij}^{\sigma} = \frac{1}{Z} \sum_s P(s) G_{ij}^{\sigma}(s). \quad (6)$$

In practice of DQMC one uses a so-called fast-update formalism to calculate the lattice Green function Eq. (4) with a single Ising spin-flip [42].

## 2.2 Continuous-time QMC

The interaction expansion (CT-INT) continuous-time quantum Monte Carlo algorithm for fermions is based on a formal series expansion for the partition function in the interaction term of the action [24]. In a schematic form with short notation  $i_k \equiv (\mathbf{r}_k, \tau_k)$  we have

$$Z = \int \mathcal{D}[c^*, c] e^{-S_0[c^*, c]} \sum_{k=0}^{\infty} \frac{(-U)^k}{k!} \int_0^{\beta} d\tau_1 \dots d\tau_k c_{i_1 \uparrow}^* c_{i_1 \uparrow} c_{i_1 \downarrow}^* c_{i_1 \downarrow} \dots c_{i_k \uparrow}^* c_{i_k \uparrow} c_{i_k \downarrow}^* c_{i_k \downarrow}, \quad (7)$$

where  $S_0$  is the Gaussian part of the action related with  $\mathcal{G}_{ij}^{\sigma}$ . In this case we can integrate-out the fermionic path integral in Eq. (7) to get the determinant of the  $k \times k$  bare Green function  $\mathcal{G}^{\sigma}$

$$Z = Z_0 \sum_{k=0}^{\infty} (-U)^k \int_0^{\beta} d\tau_1 \dots \int_{\tau_{k-1}}^{\beta} d\tau_k \prod_{\sigma} \det \mathcal{G}_k^{\sigma}. \quad (8)$$

In order to overcome a trivial sign problem related with factor  $(-U)^k$  one uses a particle-hole transformation related with a so-called  $\alpha$ -shift [24]. The CT-INT scheme performs important sampling in the space of  $k \times k$  fermionic determinants. The probability to change  $k$  to  $k+1$ -order in the Metropolis algorithm is related with ratio of the fermionic determinants [24]

$$P(k \rightarrow k+1) = \min \left( 1, \frac{\beta U}{k+1} \prod_{\sigma} \frac{(\det \mathcal{G}_{k+1}^{\sigma})}{(\det \mathcal{G}_k^{\sigma})} \right). \quad (9)$$

The optimal order of  $k$ -perturbation, which corresponds to the maximum of the distribution function of the fermionic determinants [24] for a cluster of  $N$ -sites is of the order  $k_{opt} \sim \beta N U$ . Finally, the exact reference Green function in CT-INT formalism is calculated as

$$g_{ij}^{\sigma} = \mathcal{G}_{ij}^{\sigma} - \sum_{k,k'} \mathcal{G}_{ik}^{\sigma} \cdot M_{k,k'}^{\sigma} \cdot \mathcal{G}_{k'j}^{\sigma}, \quad (10)$$

where the  $M$ -matrix is equal to the Monte Carlo average the of inverse fermionic matrix in Eq. (8).

### 3 The DF-QMC method

We start with the strong-coupling theory of the dual fermion scheme [6, 44] for the  $t-t'-U$  Hubbard model on a square lattice. There are many important works on pure strong-coupling expansions in the hopping  $t$  for Hubbard model [45–49]. The dual-fermion scheme [6] differs from the pure strong-coupling expansion in the hopping  $t$  in a very important way: it is an expansion from a reference system to the final system, or in the “difference”  $\tilde{t}$  (Fig. 3) which converges much better. The general strategy of the dual fermion approach as a strong coupling theory is related to the formally exact expansion around an arbitrary reference system [33].

#### 3.1 Real-space scheme

Let us consider a general lattice fermion model with local Hubbard-like interaction vertex  $U$ . Using the path-integral formalism the partition function of a general fermionic lattice system (Fig. 3) can be written as the functional integral over Grassmann variables  $[c^*, c]$

$$Z_\alpha = \int \mathcal{D}[c^*, c] e^{-S_\alpha[c^*, c]}. \quad (11)$$

For the super-perturbation in the lattice Monte Carlo scheme we use a general dual-fermion expansion around an arbitrary reference system within the path-integral formalism [6, 33], similar to a strong coupling expansion [47, 48]. In this case our  $N \times N$  lattice and corresponding reference systems represents an  $N \times N$ -piece cut from the infinite lattice and periodize the bare Green function  $\mathcal{G}_\alpha$ . The general lattice action for a discretized  $N_x \times N_y \times L$  space-time lattice (for the CT-INT scheme imaginary time  $\tau$  is continuous in the interval  $[0, \beta]$ ) with general interaction term reads

$$S_\alpha[c^*, c] = - \sum_{1,2} c_1^* (\mathcal{G}_\alpha)^{-1}_{12} c_2 + \frac{1}{4} \sum_{1234} U_{1234} c_1^* c_2^* c_4 c_3. \quad (12)$$

In order to keep the notation simple, it is useful to introduce the combined index  $|1\rangle \equiv |i, \tau, \sigma\rangle$  ( $i$  being the site index).

To calculate the bare propagators  $(\mathcal{G}_\alpha)_{12}$  we start from the  $N_x \times N_y$  cluster which is cut from the infinite lattice and then force translation symmetry and periodic boundary conditions on the finite  $N_x \times N_y$  system. This procedure is easy to realize in the  $k$ -space, by doing first a double Fourier transform of the bare Green function for a non-periodic  $N \times N$  cluster  $\mathcal{G}_{\mathbf{k}, \mathbf{k}'}$ , keeping only the periodic part,  $\mathcal{G}_{\mathbf{k}}^\alpha \delta_{\mathbf{k}, \mathbf{k}'}$ .

The perturbation matrix related with the difference of the one-electron part of the action is

$$\tilde{t} = \mathcal{G}_0^{-1} - \mathcal{G}_1^{-1}. \quad (13)$$

In order to formulate an expansion around the reference action  $S_0$ , we express a connection to the final action  $S \equiv S_1$  with the same local interaction in the following form

$$S[c^*, c] = S_0[c^*, c] + \sum_{12} c_1^* \tilde{t}_{12} c_2. \quad (14)$$

The main idea of the dual fermion transformation is the change of variables from strongly correlated fermions  $(c^*, c)$  to weakly correlated “dual” Grassmann fields  $(d^*, d)$  in the path integral representation for the partition function from Eq. (14), followed by a simple perturbation treatment. The new variables are introduced through a Hubbard-Stratonovich transformation with the matrix  $\tilde{t}_{12}$  in real-space (assuming Einstein summation convention over repeated indices)

$$e^{-c_1^* \tilde{t}_{12} c_2} = Z_t \int \mathcal{D}[d^*, d] e^{d_1^* \tilde{t}_{12}^{-1} d_2 + d_1^* c_1 + c_1^* d_1} \quad (15)$$

with  $Z_t = \det[-\tilde{t}]$  and we always imply matrix inversion:  $\tilde{t}_{12}^{-1} \equiv (\tilde{t}^{-1})_{12}$ . Using this transformation, the lattice partition function becomes

$$Z = Z_0 Z_t \int \mathcal{D}[c^*, c, d^*, d] e^{d_1^* \tilde{t}_{12}^{-1} d_2} \langle e^{d_1^* c_1 + c_1^* d_1} \rangle_0 \quad (16)$$

with the standard definition of average over  $S_0$

$$\langle \dots \rangle_0 = \frac{1}{Z_0} \int \mathcal{D}[c^*, c] \dots e^{-S_0[c^*, c]}. \quad (17)$$

Now we can integrate-out the  $c^*, c$  fermions and show that the average over  $S_0$  can be rewritten in the cumulant expansion [48] of connected correlators  $\langle \dots \rangle_{0c}$

$$\langle e^{d_1^* c_1 + c_1^* d_1} \rangle_0 = \exp \left[ \sum_{n=1}^{\infty} \frac{(-1)^n}{(n!)^2} \gamma_{1\dots n, n' \dots 1'}^{(2n)} d_1^* \dots d_n^* d_{n'} \dots d_{1'} \right] \quad (18)$$

with cumulant of the reference system that can be calculated within QMC

$$\gamma_{1\dots n, n' \dots 1'}^{(2n)} = (-1)^n \langle c_1 \dots c_n c_{n'}^* \dots c_{1'}^* \rangle_{0c}. \quad (19)$$

We can write the effective action for “dual fermions”  $\tilde{S}[d^*, d]$  in the lowest-order approximation for the dual interaction [7]. The first term in the cumulant expansion, Eq. (18), with  $n = 1$  ( $\gamma_{11}^{(2)}$ ), which is bilinear over the  $[d_1^*, d_2]$  Grassmann variable, corresponds to the exact Green function of the reference system

$$g_{12} = -\langle c_1 c_2^* \rangle_0 = \frac{-1}{Z_0} \int \mathcal{D}[c^*, c] c_1 c_2^* e^{-S_0[c^*, c]}. \quad (20)$$

Note, that all correlators of the reference system will be written in lowercase. Together with the term  $\tilde{t}_{12}^{-1}$  in Eq. (16) it gives the bare Green function for the dual fermions

$$\tilde{G}_{12}^0 = [\tilde{t}^{-1} - \hat{g}]_{12}^{-1}. \quad (21)$$

The second term in the cumulant expansion, Eq. (18), with  $n = 2$  ( $\gamma_{122'1'}^{(4)}$ ), which is biquadratic over the  $[d_1^*, d_2]$  Grassmann variable, gives the effective two-particle interaction among the dual-fermions. The corresponding connected four-point vertex has the form

$$\gamma_{1234} = \langle c_1 c_2 c_3^* c_4^* \rangle_0 - \langle c_1 c_4^* \rangle_0 \langle c_2 c_3^* \rangle_0 + \langle c_1 c_3^* \rangle_0 \langle c_2 c_4^* \rangle_0 \quad (22)$$

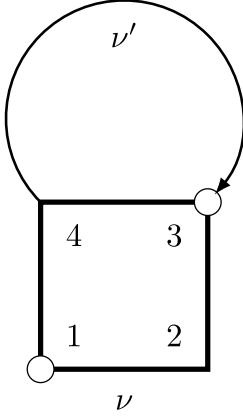


**Fig. 4:** Feynman diagram for the first-order dual fermion perturbation for the self-energy  $\tilde{\Sigma}_{12}(\nu)$ : a line represents the non-local dual Green function  $\tilde{G}_{43}(\nu')$  and a box is the two-particle vertex (cumulant)  $\gamma_{1234}$ ,  $(\sigma, \sigma')$  are spin-indices.

with four-point correlator, or two-particle Green function, for the reference system

$$\langle c_1 c_2 c_3^* c_4^* \rangle_0 = \frac{1}{Z_0} \int \mathcal{D}[c^*, c] c_1 c_2 c_3^* c_4^* e^{-S_0[c^*, c]}. \quad (23)$$

Finally, the dual-fermion action in the two-particle approximation has the form

$$\tilde{S}[d^*, d] = - \sum_{12\nu\sigma} d_{1\nu\sigma}^* (\tilde{G}_\nu^0)_{12}^{-1} d_{2\nu\sigma} + \frac{1}{4} \sum_{1234} \gamma_{1234} d_1^* d_2^* d_4 d_3. \quad (24)$$

Note, that we change sign for the interaction terms using anti-commutation rules for Grassmann variables in order to be consistent with the standard form for Coulomb interactions (Eq. (12)). The first-order correction to the dual self-energy is given by the diagram shown in Fig. 4 and can be calculated for a large system within the QMC-scheme as

$$\tilde{\Sigma}_{12}^{(1)} = \sum_{s-QMC} \sum_{3,4} \gamma_{1324}^d(s) \tilde{G}_{43}^0 \quad (25)$$

where the density vertex reads

$$\gamma_{1234}^d = \gamma_{1234}^{\uparrow\uparrow\uparrow\uparrow} + \gamma_{1234}^{\uparrow\uparrow\downarrow\downarrow}. \quad (26)$$

The main trick for practical large system computations related to the fact that within the determinant DQMC scheme using the Ising-fields  $\{s\}$  or within the CT-INT with stochastic sampling of interaction order expansion  $\{s\}$ , for two-particle correlators we can use Wick's theorem

$$\gamma_{1234}(s) \equiv \langle c_1 c_2 c_3^* c_4^* \rangle_s = \langle c_1 c_4^* \rangle_s \langle c_2 c_3^* \rangle_s - \langle c_1 c_3^* \rangle_s \langle c_2 c_4^* \rangle_s. \quad (27)$$

In order to find exact relationship between real and dual Green function, we perform a variation of  $\ln Z$  in Eq. (17) and Eqs. (11,14) with respect to  $\tilde{t}$  [50]

$$G_{12} = \frac{\delta \ln Z}{\delta \tilde{t}_{21}} = -\tilde{t}_{12}^{-1} + \tilde{t}_{13}^{-1} \tilde{G}_{34} \tilde{t}_{42}^{-1}. \quad (28)$$

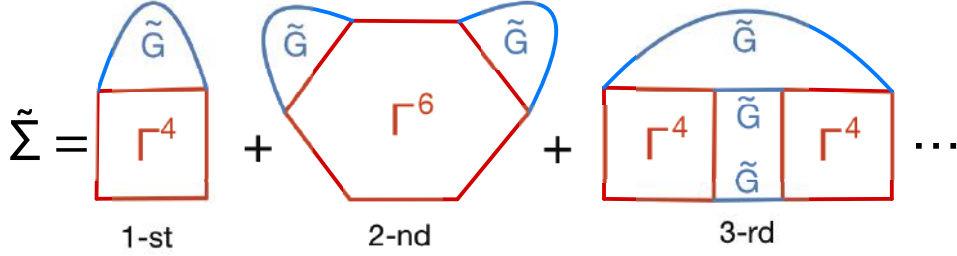


**Fig. 5:** Diagrammatic series for the dual self-energy up to the 3-rd order in the  $\tilde{G}$ .

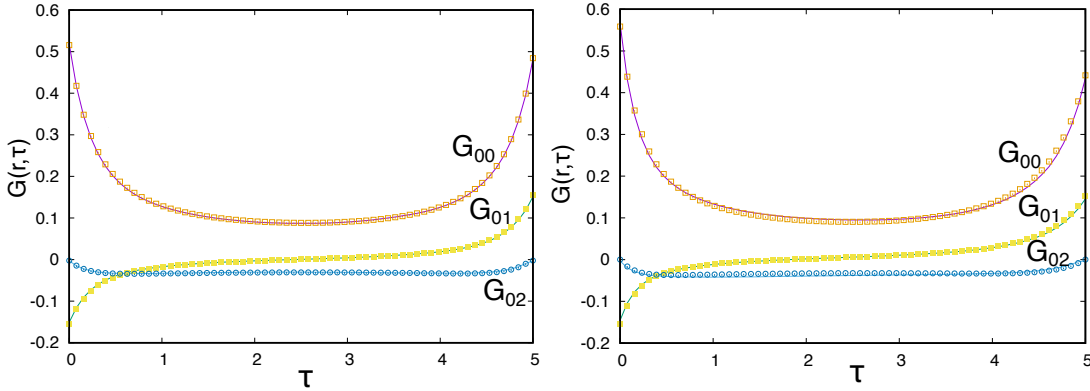


**Fig. 6:** Three non-equivalent components of the Green functions for a  $2 \times 2$  system as function of imaginary time for  $U = 5.56$ ,  $\beta = 5$  and  $t'/t = -0.1$ ,  $\mu = 0$  (left), and  $t'/t = -0.3$ ,  $\mu = -1.3$  (right). Note, that here we use the QMC definition with positive local Green function.

Using the definition of exact dual Green function  $\tilde{G}^{-1} = \tilde{G}_0^{-1} - \tilde{\Sigma}$ , we can get the expression for the real Green function

$$G_{12} = \left[ \left( g + \tilde{\Sigma} \right)^{-1} - \tilde{t} \right]_{12}^{-1}. \quad (29)$$

The dual fermion transformation allows to use arbitrary reference systems and transforms the strongly correlated lattice fermion problem to an effective action of weakly-coupled dual quasi-particles. In this case even the lowest-order approximation can give reasonable results. The exact diagrammatic series for the dual self-energy presented is in Fig. 5. The second-order diagram in  $\tilde{G}$  which includes  $\gamma^{(6)}$  is local within the cluster and can be calculated with a similar QMC scheme.

For small systems of  $2 \times 2$  clusters in the bath we can calculate the matrix of Green function of Eq. (29) directly in the real space formalism. In this case we do not need any additional periodization since the  $2 \times 2$  cluster is “self-periodic”. Since there is almost no sign problem in the DQMC method for the doped  $2 \times 2$  cluster in the bath, we can compare the first-order dual-fermion perturbation with numerically exact DQMC results. The all three non-equivalent Green functions for  $2 \times 2$  system are shown in Fig. 6, using the first-order DF-correction within the Hirsch-Fye QMC formalism. For a small perturbation,  $\Delta\mu = -0.3$  and  $\Delta t' = 0$ , a comparison with exact DQMC results (points on Fig. 6) is perfect. For a large perturbation,  $\Delta\mu = -1.5$  and  $\Delta t' = 0.15$ , one can already see small differences from the exact DQMC Green function. Nevertheless, the results of DF-QMC with only first-order corrections for the dual self-energy are very satisfactory.

### 3.2 $k$ -space scheme

For large system ( $N \geq 4$ ) it is much faster to calculate the dual self-energy in  $k$ -space with within the QMC Markov chain. The dual action in  $k$ -space reads

$$\tilde{S}[d^*, d] = - \sum_{\mathbf{k} \nu \sigma} d_{\mathbf{k} \nu \sigma}^* \tilde{G}_{0\mathbf{k}\nu}^{-1} d_{\mathbf{k} \nu \sigma} + \frac{1}{4} \sum_{1234} \gamma_{1234} d_1^* d_2^* d_3 d_4. \quad (30)$$

Using the short notation  $k \equiv (\mathbf{k}, \nu_n)$  with the fermionic Matsubara frequencies  $\nu_n = (2n+1)\pi/\beta$ ,  $n \in \mathbf{Z}$ , the dual Green function is equal to

$$\tilde{G}_k^0 = (\tilde{t}_k^{-1} - \hat{g}_k)^{-1}. \quad (31)$$

Since the bare dual Green function is calculated in the independent QMC run for the reference system, it is fully translationally invariant  $\tilde{G}_{34}^0 \equiv \tilde{G}^0(3-4)$  and we use the Fourier transform to calculate the  $k$ -space dual Green function  $\tilde{G}_k^0$ . Within the QMC Markov chain the lattice auxiliary Green function is not translationally invariant, therefore for  $g_{12}^{s\sigma} = -\langle c_{1\sigma} c_{2\sigma}^* \rangle_s$  we use the double Fourier transform to calculate  $g_{kk'}^{s\sigma}$ . Note that here we have explicitly written the fermionic spin  $\sigma$  and the auxiliary Ising spins  $s_i$ . To include the “disconnected part” of the vertex in equation Eq. (22) we just subtract the exact Green function from the previous QMC run of the paramagnetic reference system

$$\tilde{g}_{12}^{s\sigma} = g_{12}^{s\sigma} - g_{12}. \quad (32)$$

In the  $k$ -space this subtraction has the form

$$\tilde{g}_{kk'}^{s\sigma} = g_{kk'}^{s\sigma} - g_k \delta_{kk'}. \quad (33)$$

For the transformation of the vertex  $\gamma_{1234}^d$  in Eq. (26) within the QMC step in  $k$ -space we take into account that indices (3, 4) are “diagonal” in  $k$ -space due to the multiplication by the translationally invariant dual Green function  $\tilde{G}_{34}^0$ , which transforms as  $\tilde{G}_k^0 \delta_{kk'}$ , and indices (1, 2) become translationally invariant after the QMC-summation, which finally leads us to the equation for the spin-up components of the first-order dual self-energy  $\tilde{\Sigma}_k$  in the paramagnetic phase

$$\tilde{\Sigma}_k^{(1)} = \frac{-1}{(\beta N)^2 Z_{QMC}} \sum_{s-QMC} \sum_{k'} \left( \tilde{g}_{kk}^{s\uparrow} \tilde{g}_{k'k'}^{s\uparrow} - \tilde{g}_{kk'}^{s\uparrow} \tilde{g}_{k'k}^{s\uparrow} + \tilde{g}_{kk}^{s\uparrow} \tilde{g}_{k'k'}^{s\downarrow} \right) \tilde{G}_{k'}^0. \quad (34)$$

The additional normalization factor  $\frac{1}{(\beta N)^2}$  comes from the Fourier transform in  $\mathbf{k}$  and from the  $\mathbf{k}'$ -sum with  $N$  lattice sites and summation over Matsubara frequency:  $\frac{1}{\beta} \sum_{\nu'} (\dots)$ . For paramagnetic calculations we average over the two spin projections. The corresponding lattice Green function reads

$$G_k = \left[ \left( g_k + \tilde{\Sigma}_k \right)^{-1} - \tilde{t}_k \right]^{-1}. \quad (35)$$

We note that if we neglect the dual self-energy,  $\tilde{\Sigma}_k = 0$ , this approximation is equivalent to cluster-perturbation theory (CPT) [51] and was recently implemented in the DQMC scheme [52].

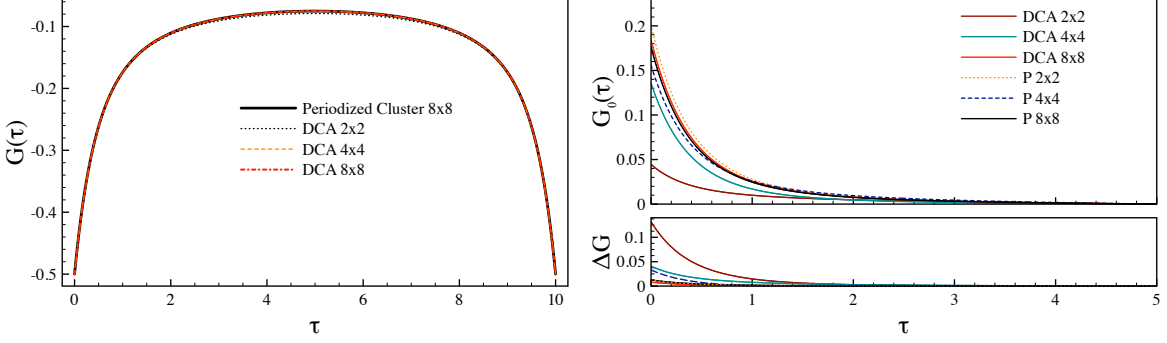


**Fig. 7:** Periodized Green function in imaginary time  $\tau$  for clusters of size  $N \times N$  with  $N = 2, 4, 8$  for our scheme compared to the DCA approach for the reference system with  $U=5.56$  and  $\beta=10$  for  $t'=0$  and  $\mu=0$ . The local Green function (left) and first nearest-neighbor (right).

Tests for different system sizes show reasonable convergence of the first-order dual-fermion approximation for small perturbations.

For practical calculations of a bare Green function for  $N_x \times N_y$  system we use a special scheme to reduce the dependence on the cluster size. We start from the non-interacting Green function with given  $t'/t$  and  $\mu$  for a infinite lattice (in practice  $50N_x \times 50N_y$  with periodic boundary conditions). We then cut the Green function to only our small  $N \times N$  system, which results in a non-periodic Green function  $\mathcal{G}_{ij}(\nu_n)$  with  $(i, j = 0, N-1)$ . In order to periodize the Green function for the small system, we average the corresponding distance, for example  $\mathcal{G}_{0,n}$  and  $\mathcal{G}_{0,N/2-n}$ . In practice, we use the “double” Fourier transform on  $i$  and  $j$  from  $\mathcal{G}_{ij}$  to  $\mathcal{G}_{kk'}$  and take the diagonal (periodic) part  $\mathcal{G}_{kk'}\delta_{kk'}$ . In this way the local Green function does not depend on the size of our cluster and the non-local part (Fig. 7) has much faster converge in comparison to the standard periodic DCA cluster scheme [53]. The reason for this fast convergence of the non-local Green function and exact local Green function is related with the real space periodization, while DCA makes the average patches in the  $k$ -space. For the  $8 \times 8$  system both periodization schemes converge for the nearest-neighbors Green function in comparison with  $16 \times 16$  ‘test’ cases (Fig.7).

We analyze the performance of the DF-QMC formalism as a function of  $\Delta\mu$  and  $\Delta t'$  for the  $4 \times 4$  periodic cluster with and without fermionic bath. The DQMC sign-problem for  $4 \times 4$  systems is also mild and we can compare our DF-QMC with numerically exact tests for the same  $\mu$  and  $t'$ . We use a value of  $U=5.56$  which corresponds to a degenerate ground state of the plaquette [19]. For all Hirsch-Fye DQMC calculations we use imaginary time discretization with  $L=64$  slices. Fig. 8(a) shows DF-QMC results for a small perturbation  $t'/t = -0.1$  and  $\beta = 5$  in comparison with exact DQMC. The agreement is very good which shows the strength of dual fermion QMC theory for a small perturbation. Next, we compare for the  $t'/t = -0.3$  case which corresponds to optimal next-nearest hopping in cuprate materials (Fig. 8(b)). In this case one can see the difference from exact DQMC results on the first Matsubara frequency, but still the overall agreement in all 6 non-equivalent  $k$ -points of the  $4 \times 4$  system is quite satisfactory. The effects of a chemical potential shift  $\mu=-0.5$  is presented in Fig. 8(c). Qualitatively, agreement between perturbative DF-QMC and exact DQMC is similar to the case of  $t'/t=-0.3$ , but the

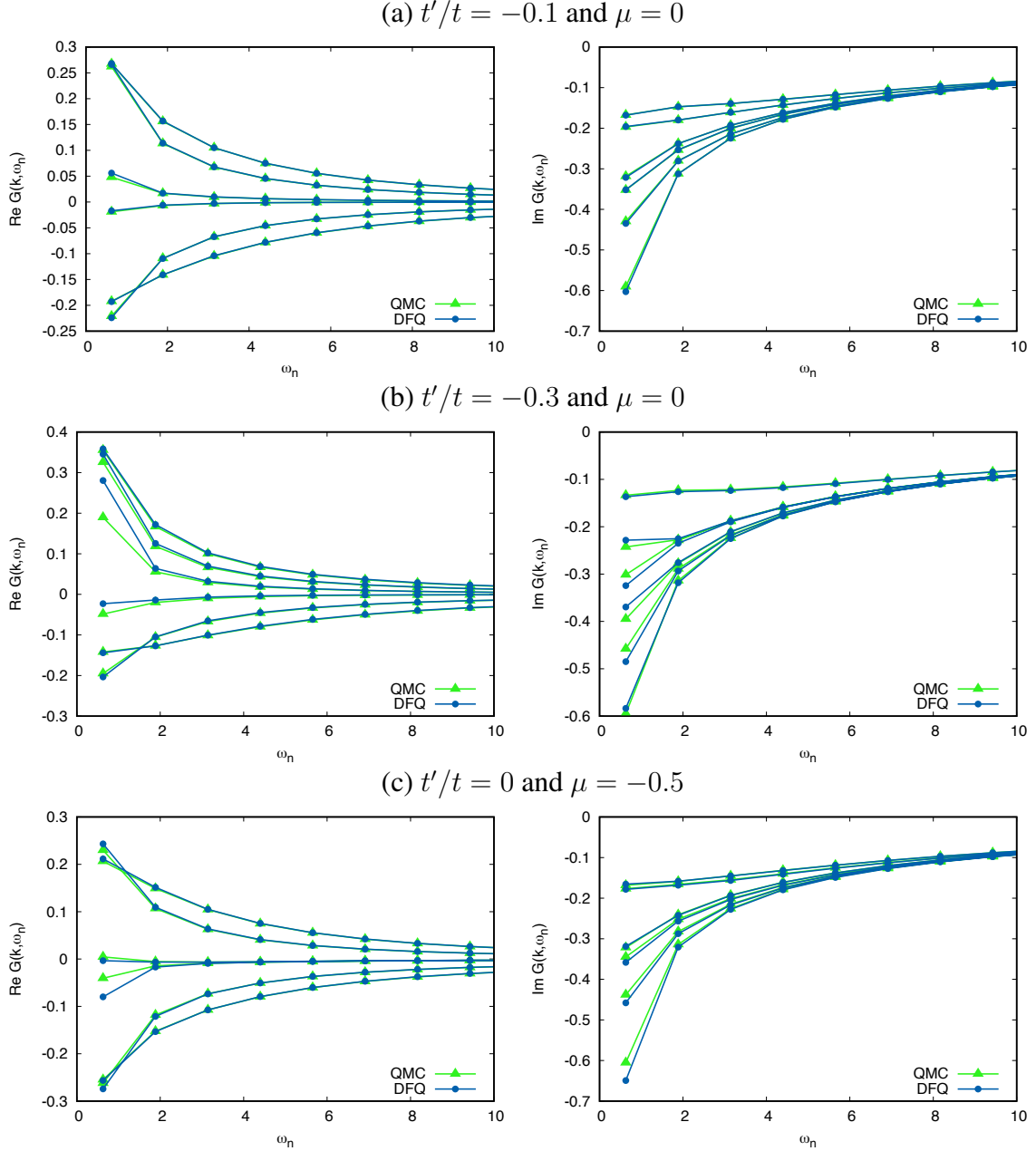


**Fig. 8:** Green functions from DF-QMC (DFQ) in comparison with numerically exact DQMC results (QMC) for the  $4 \times 4$  system in Matsubara space with  $U=5.56$ ,  $\beta=5$  and  $t'/t$ ,  $\mu$  as indicated above the plots. Real part (left) imaginary part (right).

structure of all 6 non-equivalent Green functions of the  $4 \times 4$  system is very different. Still, the dual-fermion strong coupling perturbation in  $k$ -space works reasonably well.

Fig. 9 shows the combined effect of a strong chemical-potential shift  $\mu=-1$  and next-nearest hopping  $t'/t=-0.3$ . In this case we show results of the CT-INT approach with  $\beta=10$ . The agreement is very good, and only one Green function (the lowest imaginary part) which corresponds to the  $X$ -point ( $\mathbf{k} = (\pi, \pi)$ ) and is located close to the Fermi level (the corresponding real part is close to zero) the dual perturbation shows a small discrepancy. In principle, one can reduce the error of the dual perturbation if one can choose the reference closer to the target system. The main condition is a weak sign problem for the reference system. Since this is

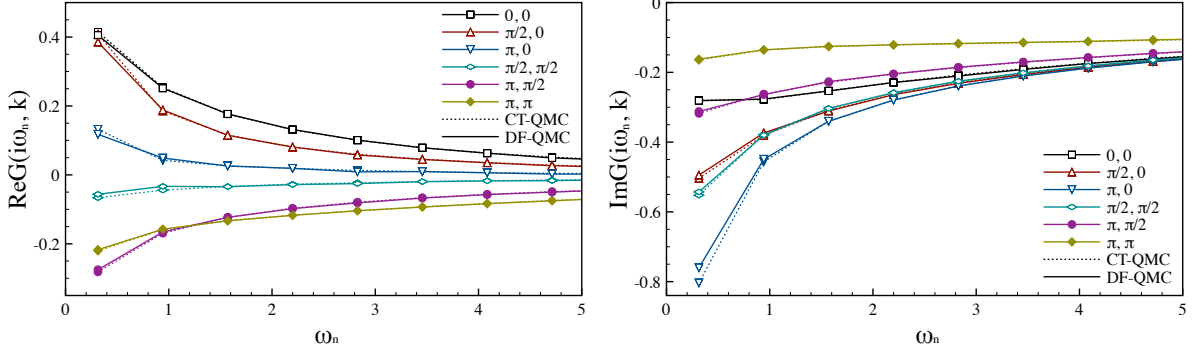


**Fig. 9:** Green functions from DF-CT-QMC (DF-QMC) in comparison with numerically exact QMC results (CT-QMC) for the  $4 \times 4$  system in Matsubara space with  $U=5.56$ ,  $t'/t=-0.3$ ,  $\mu=-1$  and  $\beta=10$ . Real part (left) and imaginary part (right).

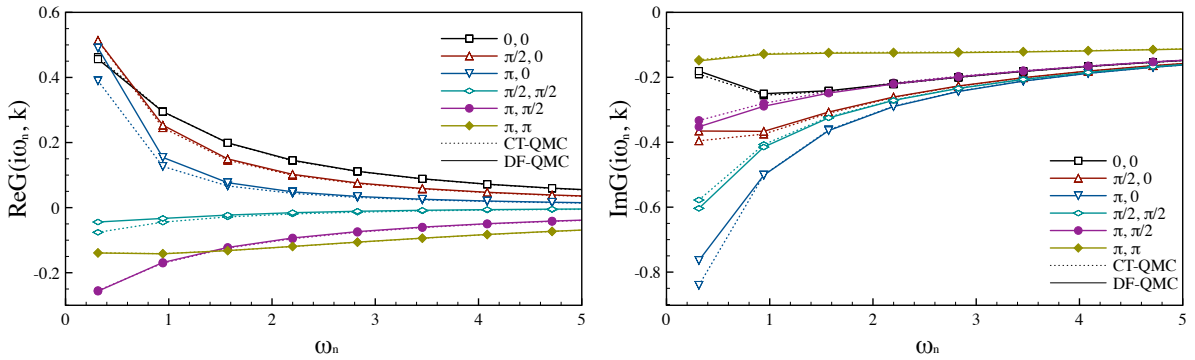


**Fig. 10:** Green functions from DF-CT-QMC (DF-QMC) perturbation for  $t'/t=-0.3$ , starting from a reference system with  $t'/t=-0.1$  in comparison with numerically exact QMC results (CT-QMC) for the  $4 \times 4$  system in Matsubara space with  $U=5.56$ ,  $\mu=0$  and  $\beta=10$ . Real part (left) and imaginary part (right).

always the case for small  $4 \times 4$  clusters, we can show in the Fig. 10 the CT-INT results starting from a reference system corresponding to  $t'/t=-0.1$  for the target system with  $t'/t=-0.3$ . In this case, for lower temperature,  $T=t/10$ , the DF-QMC results are still in a good agreement with the exact solution. This example shows that we can also use an “over-doped” Hubbard model ( $-\mu/t \simeq 4$  in Fig. 3) as a reference system in order to tackle the optimally doped case with super-QMC scheme.

## 4 Results for $8 \times 8$ lattices

For large  $8 \times 8$  systems at  $\beta = 10$ , the average sign in DQMC is of the order of  $10^{-3}$  even with a fermionic bath, and calculations of the test Green function are no longer possible. For much larger temperatures, corresponding to  $\beta=3$  and not so large  $U=5.56$  the sign problem is not severe and it is still possible to prepare a DQMC test. Fig. 11 shows a comparison of the Matsubara Green functions for all 15 non-equivalent  $k$ -points in dual-fermion perturbation with Hirsch-Fye QMC and DQMC-test. The agreement is quite good, but one should remember the very high temperature of this test ( $T=t/3$ ) which results in metallic behavior of all Green functions.

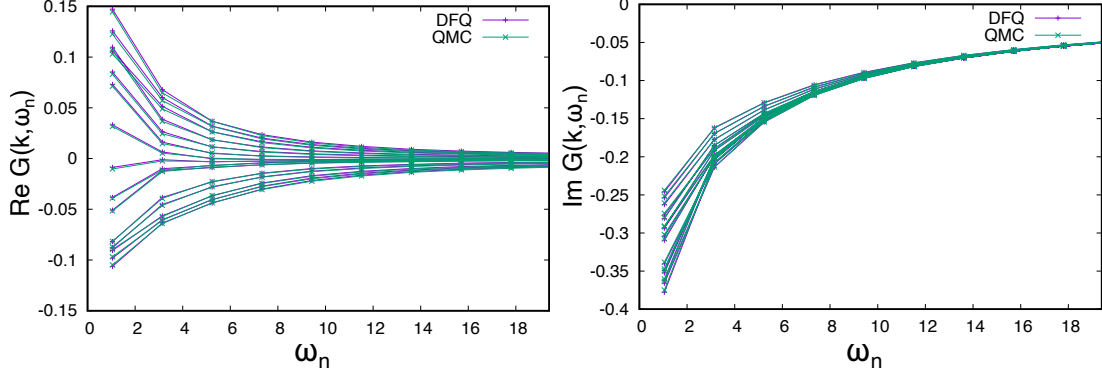


**Fig. 11:** Green function for the  $8 \times 8$  lattice with  $U = 5.56$ ,  $t'/t = -0.3$ ,  $\mu = -1.5$ ,  $\beta = 3$  for DF-QMC (DFQ) in comparison with DQMC test (QMC).

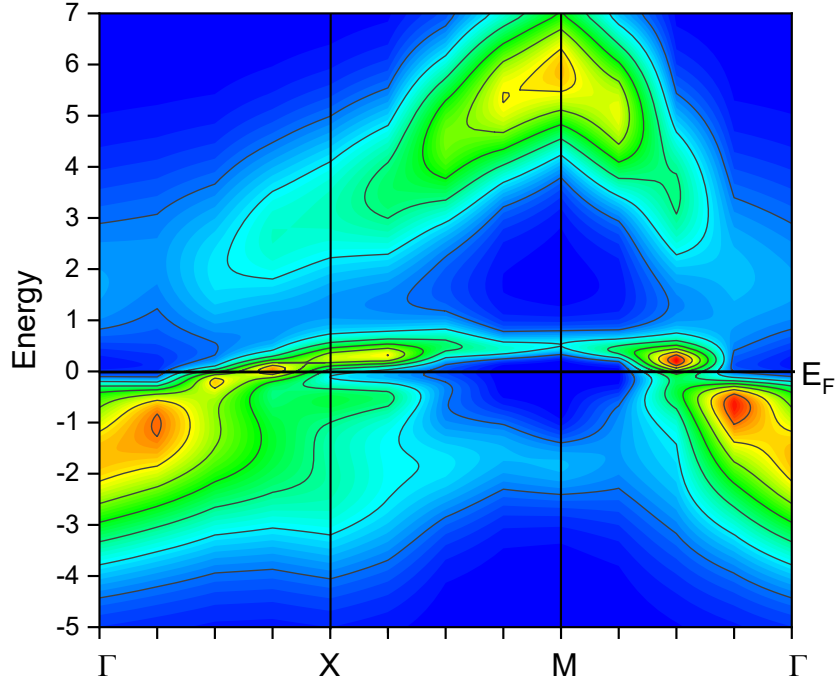


**Fig. 12:** Spectral function  $-\Im G(\mathbf{k}, \omega)/\pi$  from dual-fermion QMC (CT-INT) for a  $8 \times 8$  lattice with  $U/t = 8$ ,  $t'/t = -0.3$ ,  $\mu = -2.0$ , and  $\beta = 10$ .

We have calculated the Green function for the doped two-dimensional Hubbard model for a periodic  $8 \times 8$  system with  $U/t=8$ ,  $t'/t=-0.3$  and  $\mu/t=-2$  for  $\beta=10/t$  using a CT-INT version of the CT-QMC scheme [24]. Note that for the non-interacting Green function we used the infinite-lattice limit with periodic boundary conditions for the calculated  $8 \times 8$  system. This scheme reduces the cluster-size dependence for the bare Green function: in particular, the local one does not depend at all on the choice of the “simulation box”. On the other hand, it may underestimate the effect of  $U$ -interactions, since they appear only in the calculated cluster. This may explain a small gap in the half-filled reference system compared to a standard lattice determinant QMC scheme [40]. The results for the first-order dual-fermion perturbation from the half-filled system indicate the formation of a correlated pseudogap electronic structure. Fig. 12 shows the color map of the spectral function along the irreducible path ( $\Gamma$ - $X$ - $M$ - $\Gamma$ ) in the square Brillouin zone. For analytical continuation we used the newly developed scheme [54].

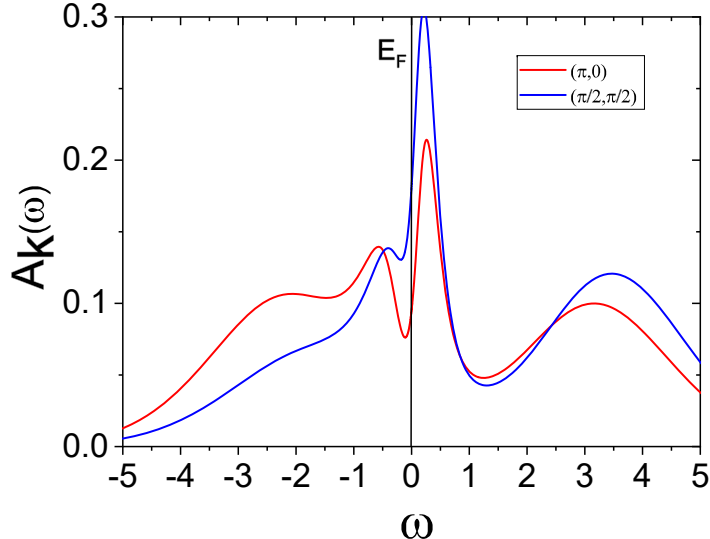


**Fig. 13:** Spectral function  $-\Im G(\mathbf{k}, \omega)/\pi$  for two different  $k$ -points corresponding to the anti-nodal  $(\pi, 0)$  and nodal  $(\pi/2, \pi/2)$  point in the dual fermion QMC (CT-INT) scheme for a  $8 \times 8$  lattice with  $U/t = 8$ ,  $t'/t = -0.3$ ,  $\mu = -2.0$  and  $\beta = 10$ .

Several characteristic features of the correlated metallic phase in generic cuprate systems can be detected: the formation of an extended pseudogap region around the  $X$ -point towards the  $M$ -point, a shadow antiferromagnetic band at energy  $-2t$  near the  $M$ -point, a strongly renormalized metallic band near the nodal point around  $(\Gamma-M)/2$ . Overall, the spectral function for  $U = W$  clearly shows strong correlation features of the electronic structure far beyond a simple renormalized band paradigm.

In order to see the pseudogap and nodal-antinodal dichotomy more clearly we plot the energy dependence of the two spectral functions at the  $X$ - and the  $(\Gamma-M)/2$ -point in the Brillouin zone (Fig. 13). While at the  $X=(\pi, 0)$ -point there is a reasonably deep pseudogap formation already at  $\beta=10$ , the nodal spectral function at  $(\Gamma-M)/2=(\pi/2, \pi/2)$  shows correlated metallic behavior. A more unusual feature of the strong-coupling spectral function in Fig. 12 is related with a “shark mouth” pseudogap dip starting at  $X$  in the direction to  $M$  until half way. One can see from the energy dependence of the spectral function in the direction of  $X-M$  (Fig. 14 (middle)) that the pseudogap splitting of the sharp quasiparticle peak at zero for the  $(X-M)/4$  point is even larger than at the  $X$ -point. The same feature was observed for a self-energy in a diagrammatic Monte Carlo (C-DET) investigation of the doped Hubbard model at  $U/t = 6$  [25]. We would like to point out that all these effects are not simply an artifact of the analytical continuation with the MaxEnt scheme and can be detected by inspection of the original complex Matsubara Green function from DF-QMC calculations (Fig. 15). If we compare the  $X=(\pi, 0)$  and  $(X-M)/4=(\pi, \pi/4)$  points then both quasiparticle peaks are located almost at the Fermi energy (the real part of  $G(\mathbf{k}, \omega_n)$  is close to zero) but the pseudogap or upturn of the imaginary part of  $G(\mathbf{k}, \omega_n)$  for the first Matsubara frequencies are more pronounced at the  $(\pi, \pi/4)$ -point. We have also checked this characteristic feature with the Hirsch-Fye QMC scheme [43] and different MaxEnt implementations. The general structure of this spectral function is similar to recent results of dynamical variational Monte Carlo schemes [29, 30].

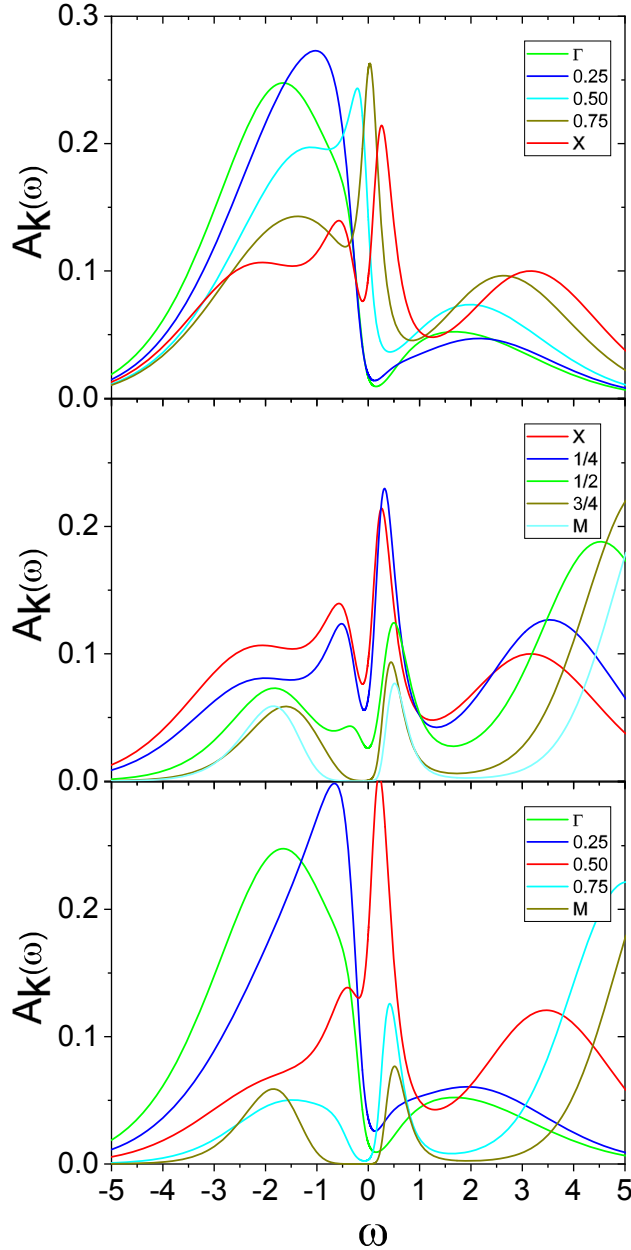


**Fig. 14:** Spectral function  $-\Im G(\mathbf{k}, \omega)/\pi$  for three different  $k$ -directions in the Brillouin Zone, (top)  $\Gamma$ - $X$ , (middle)  $X$ - $M$  and (bottom) ( $\Gamma$ - $M$ ) dual fermion QMC (CT-INT) for a  $8 \times 8$  lattice with  $U/t = 8$   $t'/t = -0.3$ ,  $\mu = -2.0$  and  $\beta = 10$ .

We plot a broadened Fermi surface using the momentum-dependent spectral function for the first Matsubara frequency (Fig. 16). Comparison with the non-interacting tight-binding Fermi surface for the same doping shows a large region of the pseudogap around the  $X$ -point and formation of Fermi arcs near the nodal point. Moreover, one can understand that the pseudogap is more pronounced a bit away from the  $X$ -point towards the  $M$ -point, where the non-interacting Fermi surface crosses the Brillouin zone. We also compare the Fermi surface plot for smaller values of  $U/t=5.6$ , which was investigated with the diagrammatic Monte Carlo technique [55,56]; this value is related to a plaquette degenerate point [19]. While the Fermi surface for small  $U/t=5.6$  agrees well with the results of the diagrammatic Monte Carlo approach [56]

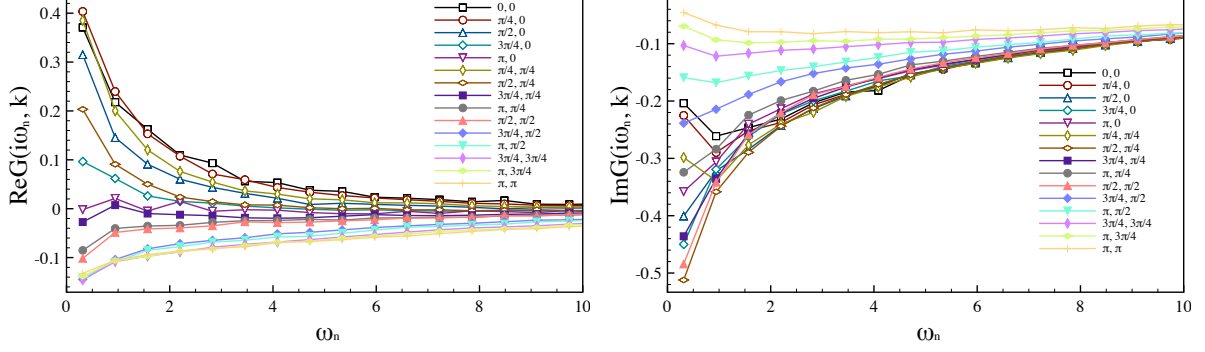


**Fig. 15:** Green function  $G(\mathbf{k}, \omega_n)$  on the Matsubara axes for all 15 non-equivalent  $k$ -points in the Brillouin Zone for  $8 \times 8$  system, (left) Real part and (right) imaginary part for dual fermion QMC (CT-INT) with  $U/t = 8$   $t'/t = -0.3$ ,  $\mu = -2.0$  and  $\beta = 10$ .

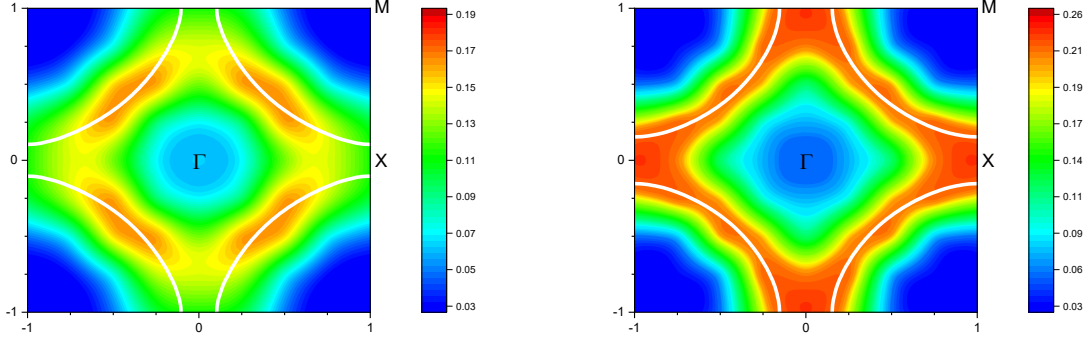


**Fig. 16:** Fermi surface of the square-lattice Hubbard model or  $k$ -dependent spectral function at the first Matsubara frequency  $-\Im G(\mathbf{k}, \omega_0)/\pi$  for dual fermion QMC (CT-INT) with  $t'/t = -0.3$ ,  $\beta = 10$  and  $U/t = 8$ ,  $\mu = -2.0$  (left)  $U/t = 5.6$ ,  $\mu = -0.9$  (right). The non-interacting Fermi surface with the same doping is shown for comparison as a white contour.

and resembles the tight-binding one with only large broadening around the  $X$ -point, the  $U/t=8$  results show already the formation of the pseudogap and Fermi arcs, that is, a nodal-antinodal dichotomy.

## 5 Discussion

We developed, for Hubbard-like correlated lattice models, the first-order strong-coupling dual fermion expansion in the shift of the chemical potential (doping) and in the second-neighbor hopping ( $t'$ ). The starting reference point corresponds to the half-filled particle-hole symmetric system which can be calculated numerically exactly, without a fermionic sign problem. For the physically interesting parameter range of cuprate-like systems (around 10% doping and  $t'/t=-0.3$  we can obtain a reasonable Green function for a periodic  $8 \times 8$  lattice for the temperature  $T=0.1t$ . The formation of the pseudogap around the antinodal  $X$ -point and the nodal-antinodal dichotomy are clearly seen in the present approach.

We would like to point out a few main reasons why such a “super-perturbation” scheme works: first of all, the reference system already contains the main correlation effects which results in the four-peak structure of the density of states for the half-filled lattice Monte Carlo calculations [40]; second, the first-order strong-coupling perturbation relies on the lattice four-point vertex  $\gamma_{1234}$  (Eq. (23)) which is obtained numerically exactly and has all the information about the spin and charge susceptibilities of the lattice; and third, if the dual perturbation Green function  $\tilde{G}_{12}^0$  (Eq. (21)) is relatively small, results will be reasonable. The complicated question of convergence for such a dual-fermion perturbation can be checked numerically by calculating the second-order contribution in  $\tilde{\Sigma}_{12}$ . For this term one needs to calculate within lattice QMC a six-point vertex  $\gamma^{(6)}$  which will be a direction of future developments. In principle, one can also discuss an instability towards antiferromagnetism or  $d$ -wave superconductivity, introducing symmetry-breaking fields [15], which we also plan to investigate.

It is worthwhile to mention that for the starting reference system we can choose not only the half-filled case, but any doped case where the sign problem is mild, so we can use a QMC calculation to expand this numerically exact solution to “Terra Incognita” regions where the sign problem is unacceptable for direct QMC calculations.

## Acknowledgements

The CT-INT part of the DF-QMC project was performed by Sergei Iskakov from the University of Michigan. We acknowledge valuable communications with Mikhail Katsnelson, Alexei Rubtsov, Evgeny Stepanov, Igor Krivenko, Richard Scalettar, Fedor Šimkovic IV, and Riccardo Rossi.

## References

- [1] D.M. Ceperley and B.J. Alder, Phys. Rev. Lett. **45**, 566 (1980)
- [2] A. Georges, G. Kotliar, W. Krauth, and M. J. Rozenberg, Rev. Mod. Phys. **68**, 13 (1996)
- [3] W. Metzner and D. Vollhardt, Phys. Rev. Lett. **62**, 324 (1989)
- [4] E. Gull, A.J. Millis, A.I. Lichtenstein, A.N. Rubtsov, M. Troyer, and P. Werner, Rev. Mod. Phys. **83**, 349 (2011)
- [5] G. Rohringer, H. Hafermann, A. Toschi, A.A. Katanin, A.E. Antipov, M.I. Katsnelson, A.I. Lichtenstein, A.N. Rubtsov, and K. Held, Rev. Mod. Phys. **90**, 025003 (2018)
- [6] A.N. Rubtsov, M.I. Katsnelson, and A.I. Lichtenstein, Phys. Rev. B **77**, 033101 (2008)
- [7] S. Iskakov, M. Katsnelson, and A. Lichtenstein, arXiv (2023)
- [8] R. Mondaini, S. Tarat, and R.T. Scalettar, Science **375**, 418 (2022)
- [9] T. Schäfer, N. Wentzell, F. Šimkovic, Y.-Y. He, C. Hille, M. Klett, C.J. Eckhardt, B. Arzhang, V. Harkov, F.-M. Le Régent, A. Kirsch, Y. Wang, A.J. Kim, E. Kozik, E.A. Stepanov, A. Kauch, S. Andergassen, P. Hansmann, D. Rohe, Y.M. Vilk, J.P.F. LeBlanc, S. Zhang, A.-M.S. Tremblay, M. Ferrero, O. Parcollet, and A. Georges, Phys. Rev. X **11**, 011058 (2021)
- [10] H. De Raedt and A. Lagendijk, Phys. Rep. **127**, 233 (1985)
- [11] E.Y. Loh, J.E. Gubernatis, R.T. Scalettar, S.R. White, D.J. Scalapino, and R.L. Sugar, Phys. Rev. B **41**, 9301 (1990)
- [12] M. Troyer and U.-J. Wiese, Phys. Rev. Lett. **94**, 170201 (2005)
- [13] H.-C. Jiang and T.P. Devereaux, Science **365**, 1424 (2019)
- [14] Y.-F. Jiang, J. Zaanen, T.P. Devereaux, and H.-C. Jiang, Phys. Rev. Res. **2**, 033073 (2020)
- [15] C.-M. Chung, M. Qin, S. Zhang, U. Schollwöck, and S.R. White, Phys. Rev. B **102**, 041106 (2020)
- [16] M. Qin, C.-M. Chung, H. Shi, E. Vitali, C. Hubig, U. Schollwöck, S.R. White, and S. Zhang, Phys. Rev. X **10**, 031016 (2020)
- [17] M. Harland, M.I. Katsnelson, and A.I. Lichtenstein, Phys. Rev. B **94**, 125133 (2016)
- [18] M. Harland, S. Brener, M.I. Katsnelson, and A.I. Lichtenstein, Phys. Rev. B **101**, 045119 (2020)

- [19] M. Danilov, E.G. C.P. van Loon, S. Brener, S. Iskakov, M.I. Katsnelson, and A.I. Lichtenstein, npj Quant. Mater. **7**, 50 (2022)
- [20] M.T. Schmid, J.-B. Morée, Y. Yamaji, and M. Imada, arXiv (2023)
- [21] H. Xu, C.-M. Chung, M. Qin, U. Schollwöck, S.R. White, and S. Zhang, arXiv (2023)
- [22] N. Prokof'ev and B. Svistunov, Phys. Rev. Lett. **99**, 250201 (2007)
- [23] R. Rossi, Phys. Rev. Lett. **119**, 045701 (2017)
- [24] A.N. Rubtsov, V.V. Savkin, and A.I. Lichtenstein, Phys. Rev. B **72**, 035122 (2005)
- [25] F. Šimkovic, R. Rossi, A. Georges, and M. Ferrero, arXiv (2022)
- [26] F. Šimkovic, R. Rossi, and M. Ferrero, Phys. Rev. Res. **4**, 043201 (2022)
- [27] R. Rossi, N. Prokof'ev, B. Svistunov, K.V. Houcke, and F. Werner, EPL (Europhys. Lett.) **118**, 10004 (2017)
- [28] A.J. Kim, N.V. Prokof'ev, B.V. Svistunov, and E. Kozik, Phys. Rev. Lett. **126**, 257001 (2021)
- [29] M. Charlebois and M. Imada, Phys. Rev. X **10**, 041023 (2020)
- [30] P. Rosenberg, D. Sénéchal, A.-M.S. Tremblay, and M. Charlebois, Phys. Rev. B **106**, 245132 (2022)
- [31] S. Sakai, M. Civelli, and M. Imada, Phys. Rev. Lett. **116**, 057003 (2016)
- [32] A. Singh, H.Y. Huang, J.D. Xie, J. Okamoto, C.T. Chen, T. Watanabe, A. Fujimori, M. Imada, and D.J. Huang, Nat. Commun. **13**, 7906 (2022)
- [33] S. Brener, E.A. Stepanov, A.N. Rubtsov, M.I. Katsnelson, and A.I. Lichtenstein, Ann. Phys. **422**, 168310 (2020)
- [34] A.A. Abrikosov, L.P. Gorkov, and I.E. Dzyaloshinski: *Methods of quantum field theory in statistical physics* (Dover, New York, 1975)
- [35] A. Georges, G. Kotliar, W. Krauth, and M.J. Rozenberg, Rev. Mod. Phys. **68**, 13 (1996)
- [36] R. Peierls, Phys. Rev. **54**, 918 (1938)
- [37] R.P. Feynman: *Statistical mechanics: A set of lectures* (Benjamin/Cummings, 1972)
- [38] N.N. Bogolyubov, Sov. Phys. Dokl. **3**, 292 (1958)
- [39] R. Scalettar, R. Noack, and R. Singh, Phys. Rev. B **44**, 10502 (1991)
- [40] D. Rost, E.V. Gorelik, F. Assaad, and N. Blümer, Phys. Rev. B **86**, 155109 (2012)

- [41] J.E. Hirsch, Phys. Rev. B **28**, 4059 (1983)
- [42] J.E. Hirsch, Phys. Rev. B **31**, 4403 (1985)
- [43] J.E. Hirsch and R.M. Fye, Phys. Rev. Lett. **56**, 2521 (1986)
- [44] H. Hafermann, S. Brener, A.N. Rubtsov, M.I. Katsnelson, and A.I. Lichtenstein, JETP Lett. **86**, 677 (2008)
- [45] S.K. Sarker, J. Phys. C: Solid State Phys. **21**, L667 (1988)
- [46] W. Metzner, Phys. Rev. B **43**, 8549 (1991)
- [47] S. Pairault, D. Sénéchal, and A.-M.S. Tremblay, Phys. Rev. Lett. **80**, 5389 (1998)
- [48] S. Pairault, Sénéchal, D., and A.-M.S. Tremblay, Eur. Phys. J. B **16**, 85 (2000)
- [49] N. Dupuis and S. Pairault, Int. J. Mod. Phys. B **14**, 2529 (2000)
- [50] S. Brener, H. Hafermann, A.N. Rubtsov, M.I. Katsnelson, and A.I. Lichtenstein, Phys. Rev. B **77**, 195105 (2008)
- [51] C. Gros and R. Valentí, Phys. Rev. B **48**, 418 (1993)
- [52] E.W. Huang, S. Ding, J. Liu, and Y. Wang, Phys. Rev. Res. **4**, L042015 (2022)
- [53] T. Maier, M. Jarrell, T. Pruschke, and M.H. Hettler, Rev. Mod. Phys. **77**, 1027 (2005)
- [54] J. Fei, C.-N. Yeh, D. Zgid, and E. Gull, Phys. Rev. B **104**, 165111 (2021)
- [55] W. Wu, M. Ferrero, A. Georges, and E. Kozik, Phys. Rev. B **96**, 041105 (2017)
- [56] R. Rossi, F. Šimkovic, and M. Ferrero, EPL (Europhys. Lett.) **132**, 11001 (2020)